A STUDY OF THE INTRODUCTION OF IONS INTO THE REGION OF STRONG FIELDS WITHIN A QUADRUPOLE MASS SPECTROMETER

By
WILSON M. BRUBAKER

BELL & HOWELL RESEARCH CENTER
360 SIERRA MADRE VILLA
PASADENA, CALIFORNIA

CONTRACT NASW-1298

THIRD
QUARTERLY PROGRESS REPORT
for the period
17 FEBRUARY 1966 TO 17 MAY 1966

NATIONAL AERONAUTICS AND SPACE ADMINISTRATION
WASHINGTON, D.C.

A STUDY OF THE INTRODUCTION OF IONS INTO THE REGION OF STRONG FIELDS WITHIN A QUADRUPOLE MASS SPECTROMETER

By
WILSON M. BRUBAKER

BELL & HOWELL RESEARCH CENTER
360 SIERRA MADRE VILLA
PASADENA, CALIFORNIA

CONTRACT NASW-1298

THIRD
QUARTERLY PROGRESS REPORT
for the period
17 FEBRUARY 1966 TO 17 MAY 1966

NATIONAL AERONAUTICS AND SPACE ADMINISTRATION
WASHINGTON, D.C.

A STUDY OF THE INTRODUCTION OF IONS INTO THE REGION OF STRONG FIELDS WITHIN A QUADRUPOLE MASS SPECTROMETER

by

Wilson M. Brubaker

ABSTRACT

29304

This project is a theoretical and experimental study of the introduction of ions into the strong fields of a quadrupole mass filter. During the third quarter experimental studies included the use of a new stainless steel rod quadrupole in place of the ceramic rod instrument used earlier. This new quadrupole resulted in reproducible performance. Alteration of the ratio of the dc to the ac fields in the entrance region increased transmitted ion currents by factors of ten to one hundred without sacrifice in resolving power.

The design of a quadrupole system with hyperbolic instead of round rods is nearly completed.

The digital computer analysis of the degradation in performance which results from the design compromise of using round instead of hyperbolic rods has been partially completed and is described to date.

TABLE OF CONTENTS

LIST OF FIGURES

Figure

INTRODUCTION

This report covers the work done by the Bell & Howell Research Center on NASA Contract NASW-1298 from 17 February 1966 through 17 May 1966 (the third quarter of the Contract).

This project is concerned with the introduction of ions into the region of strong fields in the quadrupole mass filter. During the first quarter a computer was used to study the problem and the proposed solution. The data so obtained verified that there was a serious problem, and that the proposed solution is a most effective one.

During the second quarter preliminary experimental data were obtained. These data were quite encouraging, as they showed that a good measure of the predicted improvement could be realized in the laboratory. However, the apparatus used in obtaining these data used ceramic rods with exposed surfaces on which static charges could build up. This caused the results to be somewhat erratic with respect to time. During the third quarter the quadrupole with ceramic rods has been replaced by one with stainless steel rods, with the insulating segment supports well protected from incident ions. This refinement has eliminated the random variations in the peak heights, as experienced with the ceramic rods. The preliminary data obtained with this instrument are similar to those obtained earlier.

The design of a stainless steel hyperbolic rod quadrupole is nearly finished. This will be used in a system for making direct comparisons in the operation of it and a similar quadrupole with stainless steel round rods, as is now being used.

In order to estimate the degradation in performance which results from the design compromise of using round instead of hyperbolic rods, a computer study is being made of the ion trajectories under the influence of the two fields. Since no known analytical expression is available for the potential surfaces for the case of the round rods, the computation begins with the determination of these surfaces by the relaxation method.

APPARATUS

The apparatus used for the experiments described in this report consists, essentially, of the same assembly of components described in last quarter's report. The primary difference is the quadrupole itself which is described below. The assembled apparatus is shown in block diagram form in Fig. 1.

The Quadrupole

The stainless steel rods in this quadrupole are 0.600" in diameter and 10" long. One segment 0.600" long is located at the ion entrance end of each rod. The segments are insulated from the rods in such a manner as to avoid exposure of any insulating surfaces. Electrical connections to the rods and segments are brought through the vacuum wall in a conventional manner and are shown in Fig. 2.

Ion Source and Entrance Geometry

Figure 3 shows the ion source and its position relative to the entrance aperture of the quadrupole. It is the same as is described in last quarter's report, except that a coaxial shield has been installed between the terminal aperture in the source and the entrance aperture of the quadrupole. This was done to prevent possible stray fields from disturbing the ion beam at a point where it is most vulnerable.

Radio-Frequency Oscillator and Scanning Means

Two different self-excited push-pull oscillators were used for the experiments described in this report. One provides 1.6 MHz when loaded with the capacity of the rods and segments. The other provides 2.5 MHz under the same conditions. The dc rod voltages are derived from the rectified ac potentials. The dc segment potentials are derived from a floating battery and a dual ten-turn potentiometer. Thus, during the delayed dc mode, the segments remain at a selected, fixed potential during the scanning of the ac and dc potentials on the rods.

Mass scanning is accomplished by varying all potentials in proportion (except as noted above). The incremental potential variations required

for the desired mass scan are controlled by the saw-toothed sweep voltage generated in the scanning power supply. This same saw-toothed sweep voltage is connected to the horizontal input of the x-y recorder. Thus, as in an oscilloscope display, the plotted peaks appear at predetermined points on the x axis. The mass spectrum is scanned at a rate of once in about 30 seconds.

Electrical Connections to Quadrupole

Figure 2 shows the manner in which the change from the conventional mode to the delayed dc ramp mode of operation is accomplished. Since full ac potentials are desired in these tests, fixed mica capacitors are used between the rods and the segments. The two 32-megohm resistors from the segment pairs allow a selected dc potential to be applied without disturbing the ac potential.

Secondary Emission Multiplier

The secondary emission multiplier used on the 10" segmented quadrupole is the same "venetian-blind" type as was used on the 18" quadrupole. This multiplier has a measured gain of about 2300 when supplied with -2000 volts.

Electrometer Amplifier and X-Y Recorder

The ion current detector (Fig. 4) consists of a secondary emission multiplier with leads from its essential elements brought through the vacuum wall to allow changes in external connection. When the high voltage is connected to the first dynode and the fourteenth dynode is grounded through a resistor, the ion current from the quadrupole is increased by the gain of the multiplier and is measured by the electrometer amplifier. When the high voltage supply is disconnected and the fourteenth dynode is connected to the anode, the entire structure acts as a Faraday collector. In this mode the ion current from the quadrupole is measured directly by the electrometer amplifier. The ratio of these two current measurements is the gain of the secondary emission multiplier. The electrometer amplifier and the x-y recorder were selected for data collection in preference to the previously used oscilloscope, because this combination has greater overall sensitivity and is less responsive to inherent noise in the multiplier.

EXPERIMENTAL PROCEDURE

With the apparatus assembled as illustrated in Fig. 1, tests were made comparing the performance in the conventional mode of operation with that of the delayed dc ramp mode at two frequencies. The spectrum of krypton was again chosen for the comparison tests described in this report. Two oscillators were used. One operates at 1.6 MHz and the other at 2.5 MHz.

During the tests the important auxilliary operating parameters were monitored and maintained constant. Of special interest was the partial pressure of krypton which was monitored by an independent 3" quadrupole and a strip chart recorder.

The basic data were the ion currents plotted as a function of the potentials on the rods. This was repeated for different values of the ratio of the dc to the ac potentials. From this basic data in the form of plotted mass 84 peaks, the resolving power and peak height in amperes were calculated. The resulting data were then manually plotted to show mass 84 peak current as a function of resolving power for both modes of operation. Resolving power is defined as $\frac{s}{w}$ m, where s is the distance between adjacent peaks one mass number apart, w is the width (in the same units) measured at 10% or 50% of the peak height, and m is the mass number in amu.

In order to approach optimum performance in the delayed dc ramp mode of operation, the dc voltage on the segments was adjusted to the fixed value which gave the best transmitted ion current. No attempt was made to scan this voltage as mass discrimination was not important to these tests. For the 1.6 MHz oscillator, the empirically determined best value of dc on the segments was about 7% of the dc rod voltage. For the 2.5 MHz oscillator, the segment voltage was about 22% of the dc rod voltage. In both cases the polarity for the segments remained the same as that of the rods.

EXPERIMENTAL RESULTS

General

Experiments were designed to reveal the relative peak heights at similar resolving powers when the quadrupole was operated in the two modes (conventional and delayed dc ramp). The quadrupole was excited with two different oscillators, one operating at a nominal frequency of 1.6 MHz, the other at 2.5 MHz. The resolving power is calculated from the width of the peaks at the 10% height point, and at the 50% point.

The peak heights (for mass 84 in krypton), as functions of the resolving powers, are presented as semilog plots to best reveal the differences in the two modes of operation.

Operation at 1.6 MHz

The general characteristics of the data are displayed in Fig. 5 in which the resolving power is calculated from the width of the peak at the 10% point. Note that the magnitude of the current in the delayed mode is about an order of magnitude higher than in the conventional. These preliminary data show that the obtainable resolving power under the delayed mode is considerably higher. Further, the attenuation of the peak height as the resolving power increases is much more severe for the conventional than for the delayed mode.

The same data, except that the resolving power is calculated at the 50% peak height, are presented in Fig. 6. These data show that the advantage of the delayed dc ramp mode increases at higher resolving powers.

Figure 7 shows the summary of the data obtained with the 1.6 MHz oscillator. The ratios of the currents observed in the two modes are presented as functions of the resolving powers, as calculated at the 10% and at the 50% peak heights.

Operation at 2.5 MHz

The preliminary data for the operation at 2.5 MHz, with the resolving power calculated at the 10% points of the peaks, are presented in Fig. 8. Note that the attenuation of the peak height as a function of increasing resolving power is still more severe in this case than it was at the lower frequency. In particular, as the resolving power increases from 250 to 350, the attenuation for the conventional mode is a factor of 5.5, while for the delayed dc ramp mode it is only 1.25.

Figure 9 shows the same data calculated at the 50% point. Again, the same typical differences between operation in the two modes is apparent. Note here that the obtainable resolving power is increased by 50% with the delayed dc ramp mode. Note also the very considerable difference in peak heights in the two modes.

The results of these investigations of the operation at 2.5 MHz are presented in Fig. 10. Here the ratios of the currents obtained at comparable resolving powers for the two modes are plotted as functions of resolving power. Whether the resolving power is calculated at the 10% or the 50% points, the increase in resolved ion current at high resolving powers is in excess of one hundred.

HYPERBOLIC QUADRUPOLE

The design of the hyperbolic rod quadrupole is nearing completion. Considerable flexibility has been included in this design. The support structure will be the same as that of the present round rod system. This will permit the interchange of the rods (round and hyperbolic) from one envelope to the other. An insulated segment, similar to that on each of the round rods, will be placed at the ion entrance end of each hyperbolic rod.

Procedures and techniques for generating the hyperbolic rod surfaces, suitable for this experiment, have been developed in substantial detail. A hyperbolic layout will be made on a 50:1 scale. This will be used as a master on a pantograph-type reduction transfer to generate a positive hyperbola on a tungsten carbide wheel. This wheel will be used to crush-form a negative on the grinding wheel which in turn will be used to form-grind the hyperbolic rods. To assure the contour stability of the grinding wheel, it will be touched up periodically by contact with the tungsten carbide wheel which will be mounted directly on the grinding machine.

The hyperbolic rods will have a cross section of about 0.6" x 1.25". They will be supported by a special fixture during the grinding operation. The rod-positioning surfaces on this fixture will be ground in place on the same machine which will be used to grind the hyperbola. This procedure is expected to result in rods with surfaces of high contour accuracy.

It is anticipated that one-half of the hyperbola will be ground at a time. The rod will then be indexed end to end and the other half of the hyperbola ground. This indexing will be repeated several times on each rod to assure uniformity of the halves and the centering of the hyperbola on the rod. This is essential since the physical location of the rods is governed by the side surfaces of the rods. Further, these side surfaces are to be used as references for checking before and after final assembly.

COMPUTER STUDIES

This section was written by Thomas Harris, of Optical Research Associates. It describes the method being used by Optical Research Associates for the determination of the fields for the case of the round rod quadrupole structure. When this phase of the computer studies is completed, ion trajectories will be traced in these fields. The amplitudes of these trajectories will be compared to those in the hyperbolic structure with other conditions being similar.

STUDY OF QUADRUPOLE DETERIORATION DUE TO THE USE OF ROUND, RATHER THAN HYPERBOLIC, FIELD-FORMING SURFACES

This computer study is to determine the effect of using round rods instead of the theoretically desirable hyperbolic surfaces.

I. Representation of the Perturbation

With hyperbolic surfaces the potential throughout the space between the field-forming surfaces is given by the equation,

$$V = (V_{dc} + V_{ac} \cos \omega t)(x^2-y^2)/r_o^2$$

This has been converted to the equations for ion motion:

$$\ddot{x} = \frac{e}{M} E_x = \frac{-e}{M} \frac{\partial V}{\partial x}$$

$$\ddot{y} = \frac{e}{M} E_y = \frac{-e}{M} \frac{\partial V}{\partial y}$$

which lead to,

$$\ddot{x} = \frac{-e}{M} (V_{dc} + V_{ac} \cos \omega t)(\frac{2x}{r_o^2})$$

$$\ddot{y} = \frac{-e}{M} (V_{dc} + V_{ac} \cos \omega t)(\frac{-2y}{r_o^2})$$

These equations can be converted to the standard Mathieu Equation as has been done in previous reports. To give the trajectories included in the first quarterly report, these two equations were integrated numerically; note the independence of the x and y variables.

The introduction of circular rods instead of hyperbolic surfaces perturbs the hyperbolic potential distribution. The form of this perturbation conceivably could be a power series and, if suitable in form, could be used to trace trajectories through the perturbed fields. The conditions which such a potential function should have are the following:

1. Symmetrical in x (even order).
2. Symmetrical in y (even order).
3. When $x = \pm y$, $V = 0$ and, ideally:
4. $\frac{\partial V}{\partial x}$ independent of y.
5. $\frac{\partial V}{\partial y}$ independent of x.

One such equation would be:

$$V = \frac{(V_{dc} + V_{ac} \cos \omega t)}{r_o^2} \left[(x^2 - y^2) + a(x^4 - y^4) + b(x^6 - y^6) + c(x^8 - y^8) \times \ldots \right]$$

Once the perturbation coefficients a, b, c, ... are known, the resulting differential equations of motion:

$$\ddot{x} = \frac{-e}{M} \frac{(V_{dc} + V_{ac} \cos \omega t)}{r_o^2} \left[2x + 4ax^3 + 6bx^5 + 8cx^7 + \ldots \right]$$

$$\ddot{y} = \frac{e}{M} \frac{(V_{dc} + V_{ac} \cos \omega t)}{r_o^2} \left[2y + 4ay^3 + 6by^5 + 8cy^7 + \ldots \right]$$

can be numerically integrated, as before, to give the required trajectories.

The principal remaining problem is to find the coefficients a, b, c, ...; this is to be done by a two-step process. First, a representation of the true potential distribution must be found; second, the chosen potential function such as the one above must be filled to this true potential distribution, determining a, b, c, ... to give the best fit.

II. Finding the True Potential Distribution

There are a number of analogs of an electrostatic potential distribution which satisfy the Laplace Equation:

$$\frac{\partial^2 V}{\partial x^2} + \frac{\partial^2 V}{\partial y^2} = 0;$$

this equation must be satisfied by any process which is used to obtain the potential distribution. Two of the analogs which have been used in experimental work are the rubber-dam model and the electrolytic plotting tank. Analogs such as these give insufficient accuracy for determination of perturbations. Therefore, a computational analog, the Liebmann Method* will be used on a digital computer.

A. The Liebmann Procedure - Definition of Boundaries. - This consists of overlaying a computational model of the electrode structure with a grid of discrete points at which the potential values are to be adjusted repeatedly until no significant change takes place. The values of potential thereby obtained will satisfy the Laplace Equation. The finer the grid, the more accurate will be the final curve fitting; however, the computing cost will be increased also. It is, therefore, important to recognize that there is an eightfold symmetry in the electrode structure which requires that the computation be carried out only over the area shown in Fig. A, enclosed by the solid lines. The computational processes can be set up to recognize the fact that the potential distribution in the -y direction is only a reflection of that in the +y direction. However, the open end along the line $x = x_{max}$ presents a problem. Either a particular distribution along this line must be assumed or a particular value of E_x $(\frac{\partial V}{\partial x})$ must be assumed. The latter is less restrictive on the accuracy of the process and has been used in the ensuing program.

In the region near the origin the equipotential lines will be nearly the hyperbolic surfaces required by the quadrupole theory. As we move out toward any rods, the equipotential line shape will be dominated by the nearest rods. We could, therefore, assume that, for the region shown as the open end, the values of $\frac{\partial V}{\partial x}$ are similar to those for a circular conductor; however, the equipotential lines for such a conductor are concentric circles--a form which obviously would match the distribution very poorly near the grounded plane. The grounded plane should be a member of the set of equipotential lines. Fortunately, there is a better approximation which satisfies

---

*Zworykin, V. K. et al.: Electron Optics and the Electron Microscopes, John Wiley & Sons, Inc., pp. 386-388.

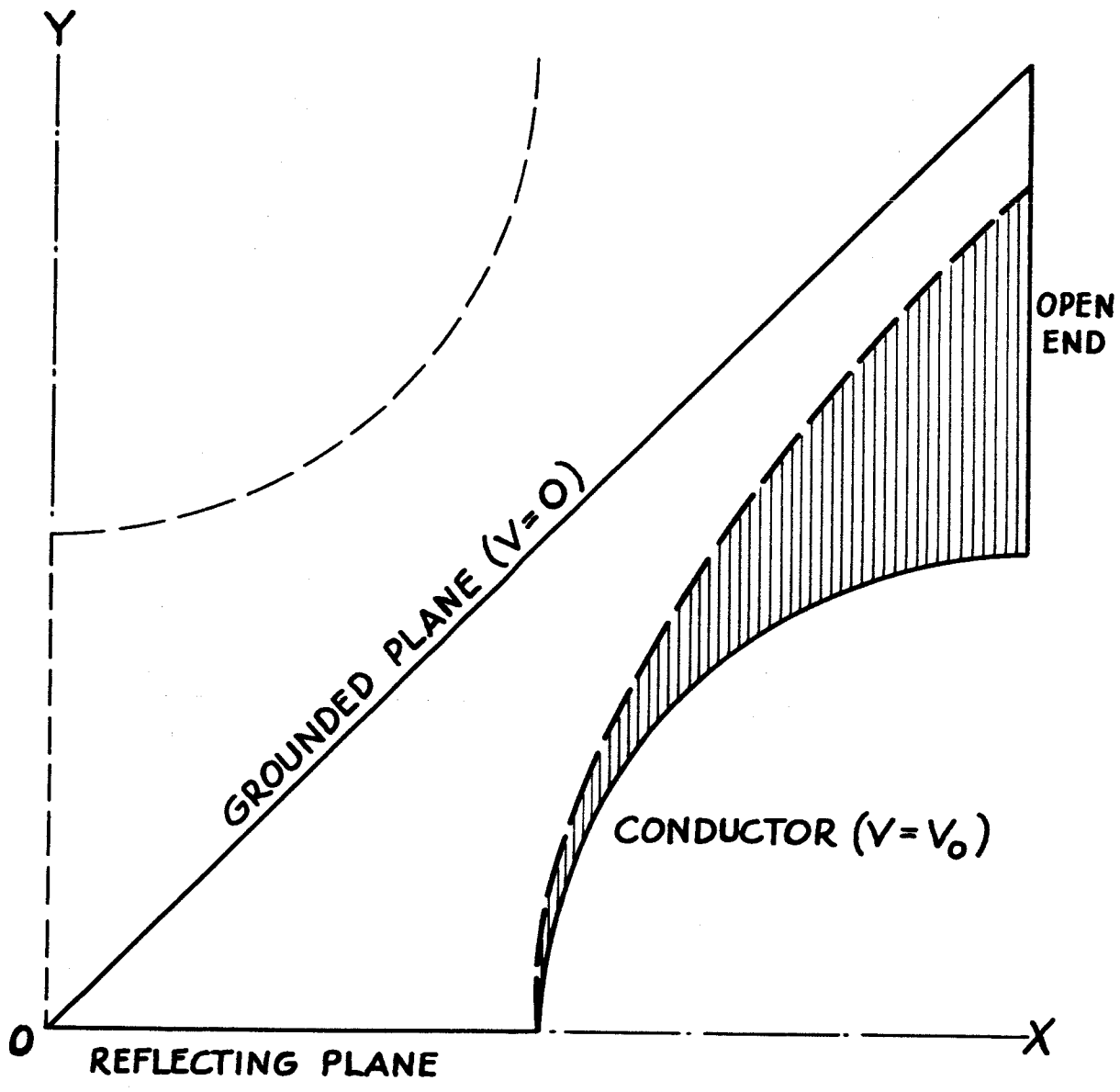

BOUNDARY CONDITIONS FOR LIEBMANN PROCEDURE

FIGURE A

this condition and which can be put in analytic form. This is for the potential distribution associated with two parallel cylindrical conductors; the equipotential lines are circles with displaced centers and include one of infinite radius coinciding with the grounded plane. The equation for potential* is, when translated to the coordinates under consideration, the following:

$$V = \left[\frac{V_o}{2 \ln\left(\frac{x_c + b}{\sqrt{2}\,R}\right)}\right] \ln\left[\frac{(x-y-b)^2 + (x+y-x_c)^2}{(x-y+b)^2 + (x+y-x_c)^2}\right]$$

where V_o = potential of the conducting rod
R = radius of the conducting rod
x_c = X coordinate of the center of the conducting rod
$b = \sqrt{x_c^2 - 2R^2}$

As mentioned before, to assume this distribution as a boundary condition would introduce a possibly inaccurate assumption. Instead, only the slope of this distribution will be assumed and only for the X-direction. This is given by,

$$\frac{dV}{dx} = \frac{V_o}{\ln\left(\frac{x_c+b}{\sqrt{2R}}\right)} \left[\frac{(x-b) + (x-x_c)}{(x-y-b)^2 + (x+y-x_c)^2} - \frac{(x+b) + (x-x_c)}{(x-y+b)^2\ (+x+y-x_c)^2}\right]$$

Using this to represent the desired slope, in the X-direction at the open end will allow the slope in the Y-direction to be determined without imposing any artificial conditions. With the open end, defined, one of the requirements of the Liebmann procedure has been met--namely that it must be applied over a closed region.

B. Starting Potential Distribution. - A second requirement is that an initial potential distribution must be provided. The closer this distribution is to the final distribution, the shorter the computation time will be. It is, therefore, important that the starting distribution be reasonable. Several have been considered, as follows:

1. Hyperbolic Form. Since the quadrupole theory says that hyperbolic equipotential surfaces are required, it is natural to try:

---

*Ramo, S.; and Whinnery, J. R.: Fields and Waves in Modern Radio, John Wiley & Sons, Inc., pp. 138-140.

$$V = \frac{V_o}{r_o^2} (x^2-y^2)$$

Although this matches what the final distribution is expected to be near the grounded plane, it matches poorly near the conducting rod. In fact, in the shaded area of Fig. A, V is greater than V_o, the potential of the rod; this is obviously impossible.

2. Hyperbolic Form with Plateau. An easy improvement over the hyperbolic form would be all values of V greater than V_o be set equal to V_o. In other words, the shaded region of Fig. A would have its potential set to V_o. This still leaves a significant change to be made by the Liebmann procedure.

3. Hyperbolic Form with Parabolic Fall-off from Cylinder Edge. A cross section with $x = c$ in the region between the cylinder and the origin shows that:

$$V = K - \frac{V_o}{r_o^2} y^2;$$

thus there is a parabolic fall-off in the y-direction. This suggests that a parabolic fall-off from the edge of the cylinder would be an improved representation. Although this is true, this implies that there is no sharp edge to the distribution in the y-direction at the edge of the conductor--that is, the slope of V is 0 in the y-direction at the edge of the conductor; this is not consistent with a physical understanding of what the final distribution ought to be.

4. Hypberbolic Form with Parabolic Fall-off from X-Axis. This last objection can be removed by centering the parabolas about the x-axis so that the skirt of the parabola describes the fall-off. In other words, from the origin out to the cylinder ($x = x_c - R$) the hyperbolic distribution is used:

$$V = \frac{V_o}{r_o^2} (x^2-y^2)$$

From the edge of the cylinder:

$$V = V_o \left[\frac{Y_{max}^2 - y^2}{Y_{max}^2 - Y_{min}^2} \right]$$

where Y_{max} = the y value of the grounded plane (=x),
Y_{min} = the y value of the cylinder edge ($= \sqrt{R^2 - (x-x_c)^2}$);
or

$$V = V_o \left[\frac{x^2-y^2}{x^2 - R^2 + (x-x_c)^2} \right]$$

This can readily be shown to be continuous with the hyperbolic distribution. Thus, a reasonable starting distribution has been obtained.

III. Fitting the Polynomial to the Distribution

Once the potential distribution has been determined, it could be used to trace trajectories directly by integration processes. However, this would be quite expensive and inaccurate. For this reason, it is best to fit a function such as the polynomial previously discussed. This is done with the least-squares method using an equation such as,

$$A_{1i}z_1 + A_{2i}z_2 + A_{3i}z_3 + A_{4i}z_4 = V_i$$

where z_1, z_2, z_3 ... are the coefficients a, b, c, ... of the chosen polynomial--the values of which must be determined. For each point (i) in the grid, there is an associated value of V_i as well as the coordinates x_i and y_i. The value of A_{1i} is the function of V_o, r_o, x_i, and y_i which multiplies the coefficient a in the chosen polynomial; the other terms (A_{2i}, A_{3i} ...) are the corresponding multipliers of b, c, ...

If these equations are set up for all the points in the grid, a matrix equation can be formed:

$$Az = V$$

which includes all equations. If then this is premultiplied by the transpose of A, we get:

$$A^TAz = A^TV$$

which is a problem consisting of four equations in four unknowns (for the above example) which, when solved, will give a least-squares fit of the coefficients to the potential distribution. With the large number of equations available to form A, the fit should be very smooth.

IV. Status of Program

Programming has proceeded through several stages as of the date of this report. These are:

1. Layout of major logic flow and planning of memory--up to more than 4000 points can be used in the grid for the Liebmann process, if necessary.

2. Programming and checkout of the following sections:

   a) Data entry and checking.
   b) Initial potential distribution calculation (as outlined in IIB).
   c) Computation of open-end gradients.
   d) Initialization of control matrix to guide Liebmann method.
   e) Liebmann procedure including interior points, reflecting plane, open end, and points adjacent to cylinder.

Remaining work includes the main control routine for the Liebmann procedure, the curve fitting, and the trajectory tracing.

CONCLUSIONS

The data reported this quarter were obtained with a quadrupole which has stainless steel rods, instead of ceramic ones. The data were reproducible, indicating that the previously noted variability was properly blamed upon the insulating surfaces of the ceramic rods.

The data obtained with the stainless steel rods are quite similar to that found before. The reduction of the ratio of the dc to the ac fields in the entrance region through the application of minimal amounts of dc potentials (and full ac potentials) to the short rod segments makes a profound difference in the operation of the quadrupole. These differences may be summarized as:

1. At the same resolving power, and with no changes other than the magnitude of the dc potential applied to the short rod segment, the transmitted ion current is increased by factors between 10 and 100.

2. The obtainable limiting resolving power is increased by factors of 10 to 50%.

3. The rate at which the peak heights change with resolving power is reduced by factors up to four. This improves analytical accuracy.

Because the use of the delayed dc ramp greatly reduces the loss of ions to the rods, it tends to produce peaks with less sharp tops. The heights of peaks with the more rounded contours are less influenced by small changes in the dc/ac voltage ratio than are those with sharp, pointed tops. This gives greater analytical accuracy.

Theory predicts and experience verifies that as the resolving power is increased, the manner in which ions approach the quadrupole becomes of increasing importance. It is anticipated that this phase of the quadrupole performance will be studied and refined in the continuation of this work.

NEXT QUARTER'S ACTIVITIES

During the fourth quarter the hyperbolic rod quadrupole will be fabricated and assembled. The system to which this is attached will in include a similar quadrupole with round rods. The excitation circuitry will either be in common for the two, or will be duplicate units. In this manner, the differences in the operation of the round and the hyperbolic quadrupoles will be explored under conditions in which the rod contours are the only known differences.

There is much more to be learned from the study of entrance conditions. As time permits, the value of the delayed dc ramp mode of operation will be observed while the following variables are changed:

1. Entrance aperture size.
2. Mass number of transmitted ions.
3. Voltage excitation level.
4. Incident ion energy.

In the preliminary data taken so far, the relative peak heights have been observed in arbitrary units. Through the use of the auxiliary 3" quadrupole the pressure of the gas used will be monitored on an absolute scale. In this manner, specific sensitivity values will be observed. This will make the future data more meaningful.

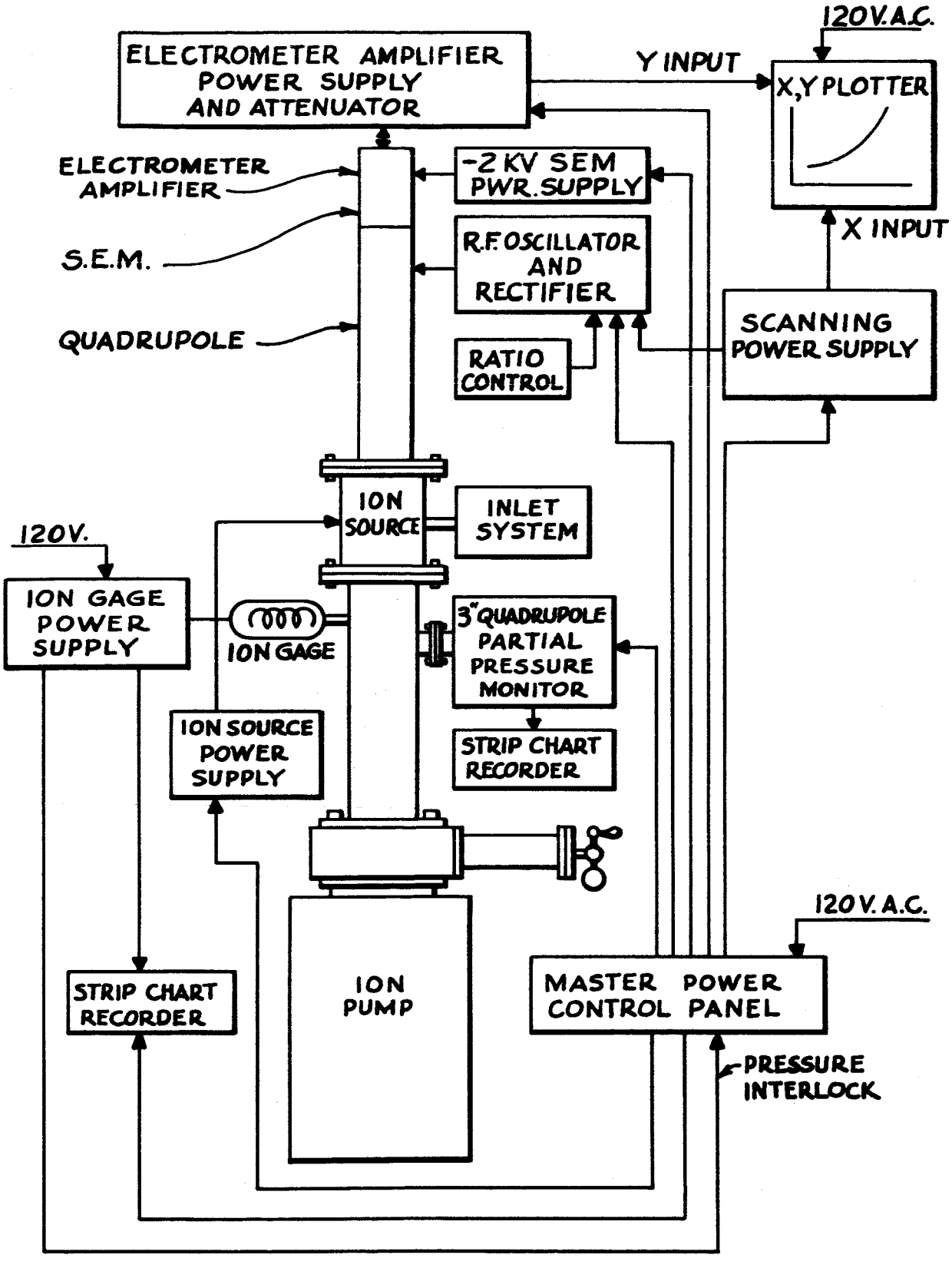

APPARATUS BLOCK DIAGRAM

FIGURE 1

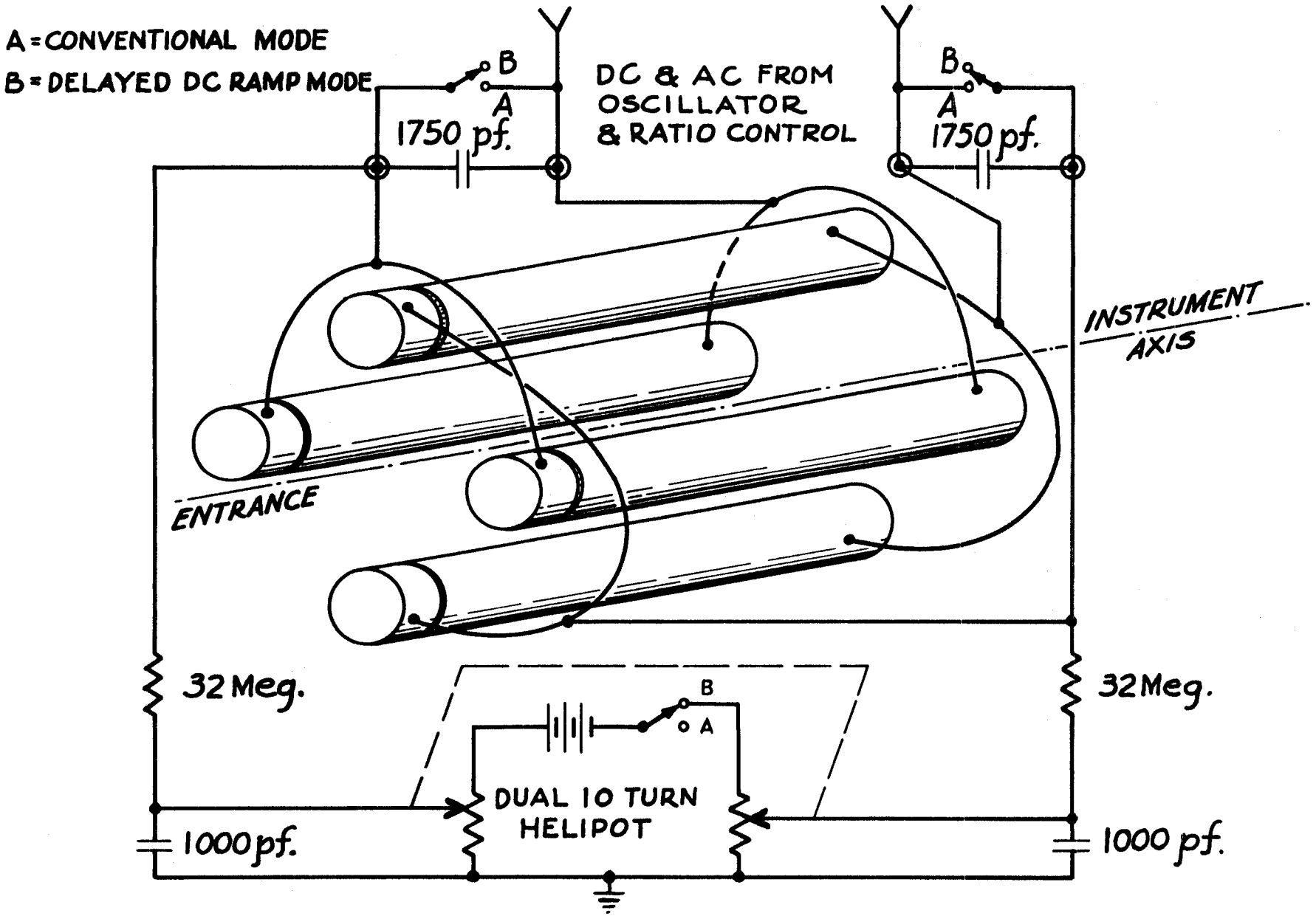

ROD SEGMENT VOLTAGE CONTROL CIRCUIT

FIGURE 2

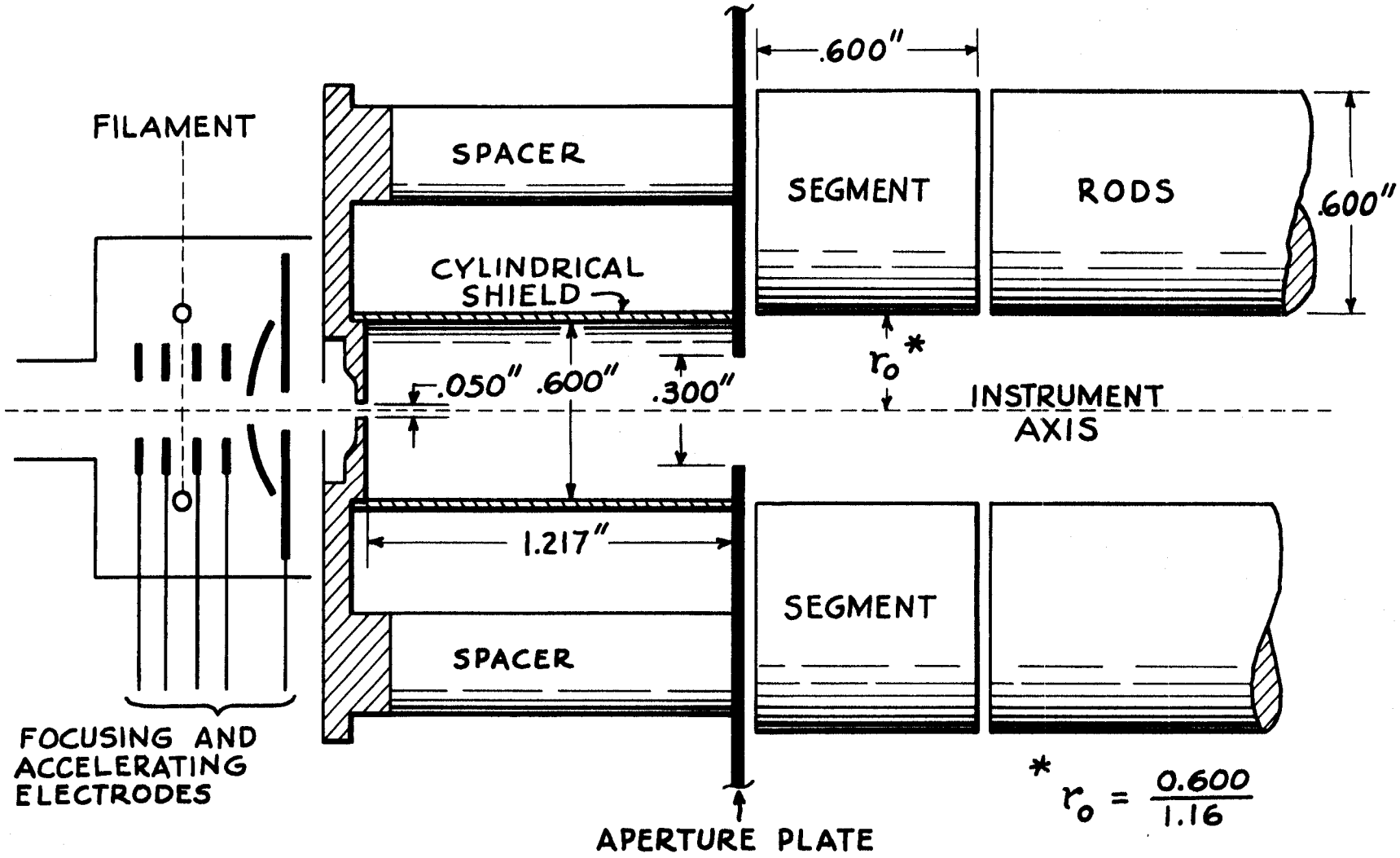

ION SOURCE & ENTRANCE GEOMETRY

FIGURE 3

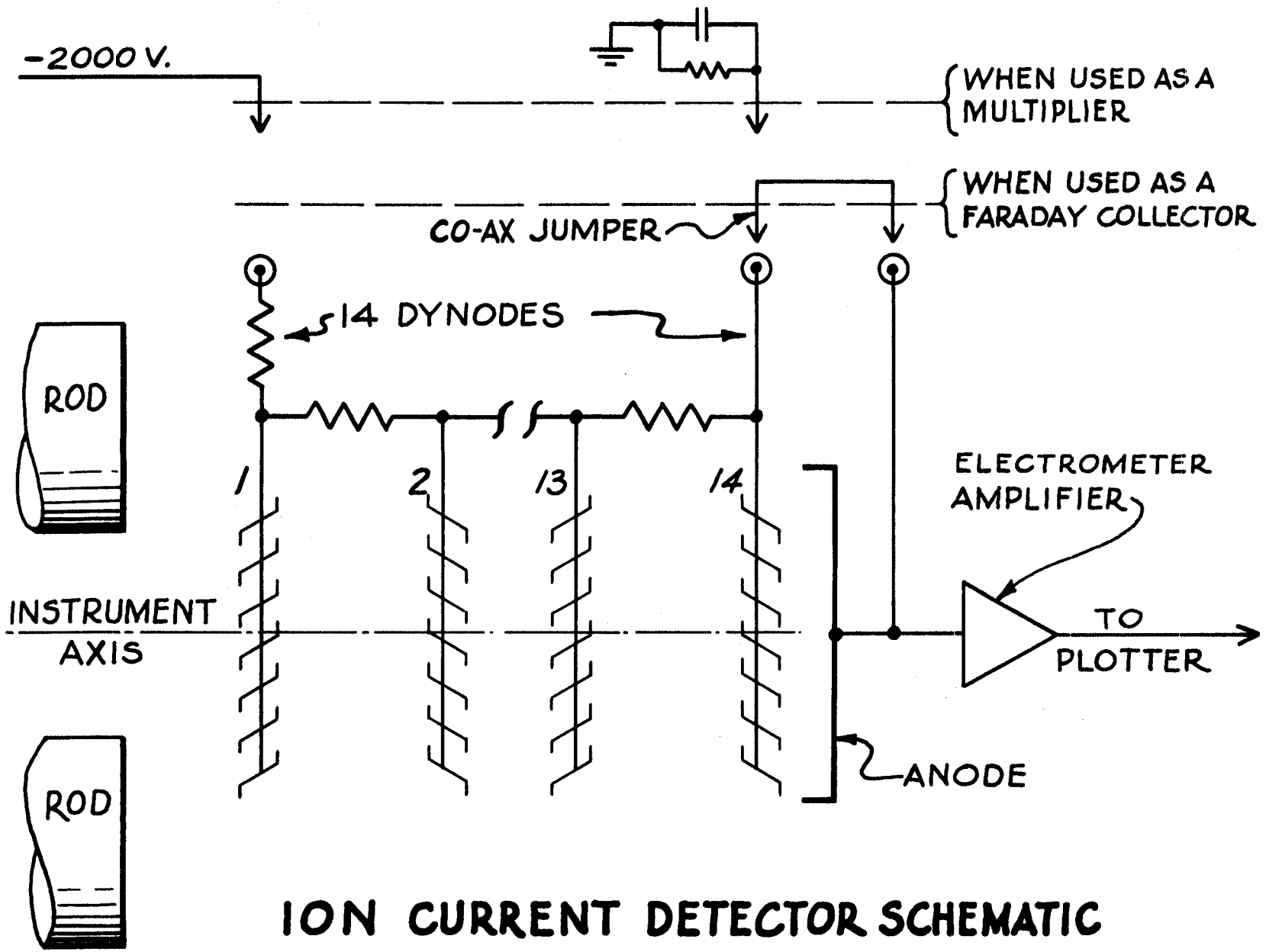

ION CURRENT DETECTOR SCHEMATIC

FIGURE 4

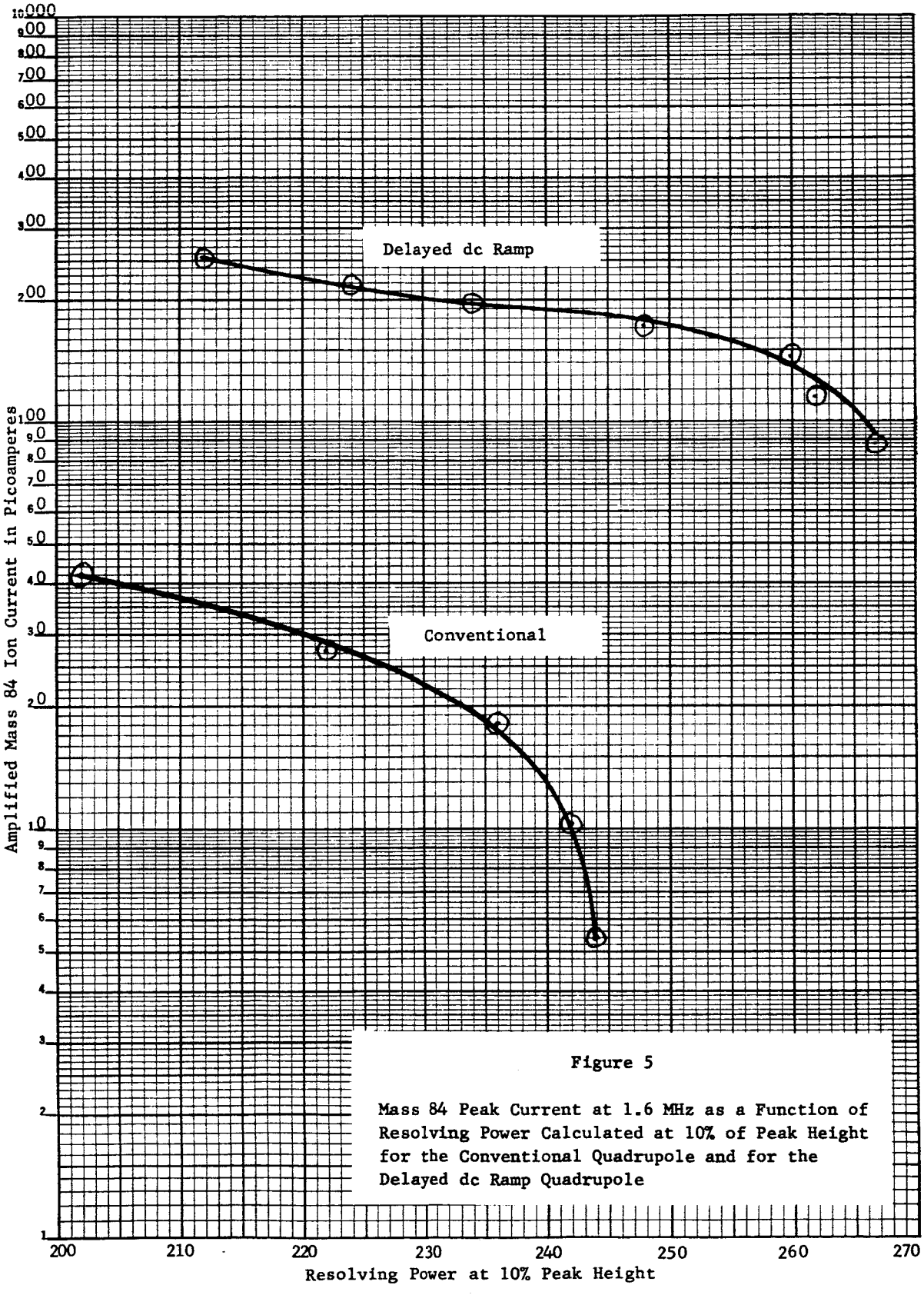

Figure 5

Mass 84 Peak Current at 1.6 MHz as a Function of Resolving Power Calculated at 10% of Peak Height for the Conventional Quadrupole and for the Delayed dc Ramp Quadrupole

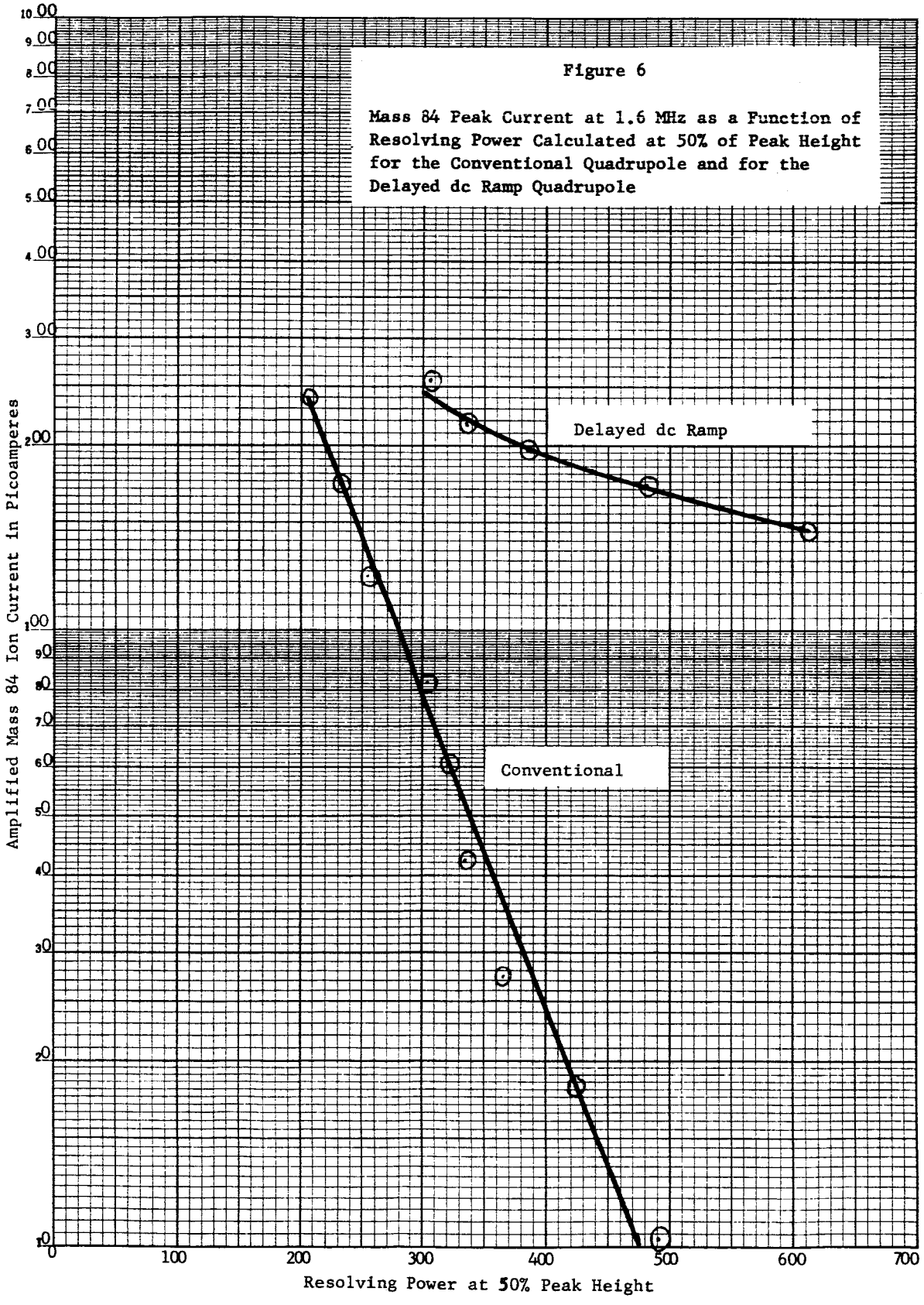
Figure 6
Mass 84 Peak Current at 1.6 MHz as a Function of Resolving Power Calculated at 50% of Peak Height for the Conventional Quadrupole and for the Delayed dc Ramp Quadrupole
Delayed dc Ramp
Conventional
Amplified Mass 84 Ion Current in Picoamperes
Resolving Power at 50% Peak Height
10 00
9 00
8 00
7 00
6 00
5 00
4 00
3 00
2 00
100
90
80
70
60
50
40
30
20
10
0
100
200
300
400
500
600
700

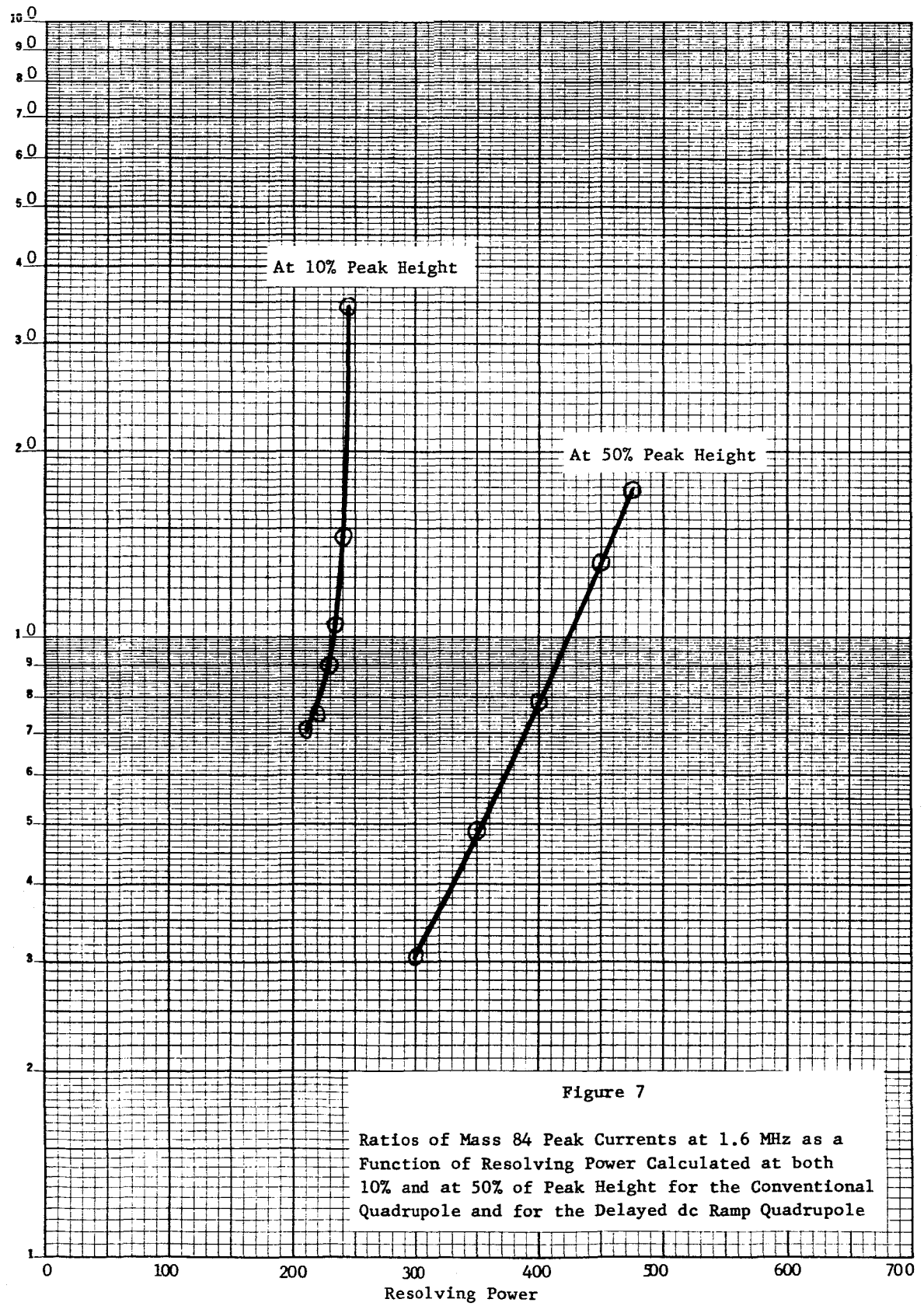

Figure 7

Ratios of Mass 84 Peak Currents at 1.6 MHz as a Function of Resolving Power Calculated at both 10% and at 50% of Peak Height for the Conventional Quadrupole and for the Delayed dc Ramp Quadrupole

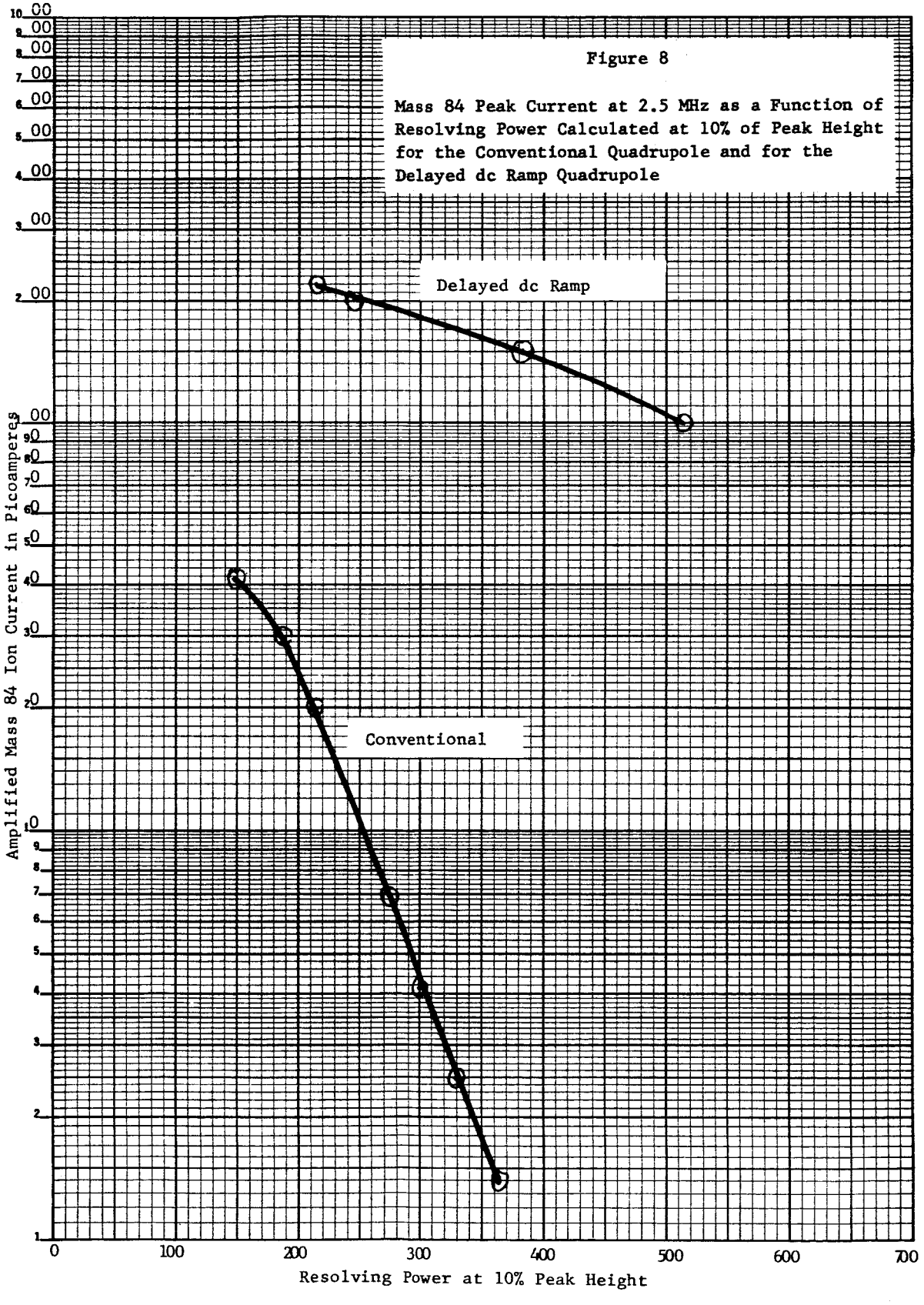
Figure 8
Mass 84 Peak Current at 2.5 MHz as a Function of Resolving Power Calculated at 10% of Peak Height for the Conventional Quadrupole and for the Delayed dc Ramp Quadrupole
Delayed dc Ramp
Conventional
Amplified Mass 84 Ion Current in Picoamperes
Resolving Power at 10% Peak Height
0
100
200
300
400
500
600
700

Figure 9

Mass 84 Peak Current at 2.5 MHz as a Function of Resolving Power Calculated at 50% of Peak Height for the Conventional Quadrupole and for the Delayed dc Ramp Quadrupole

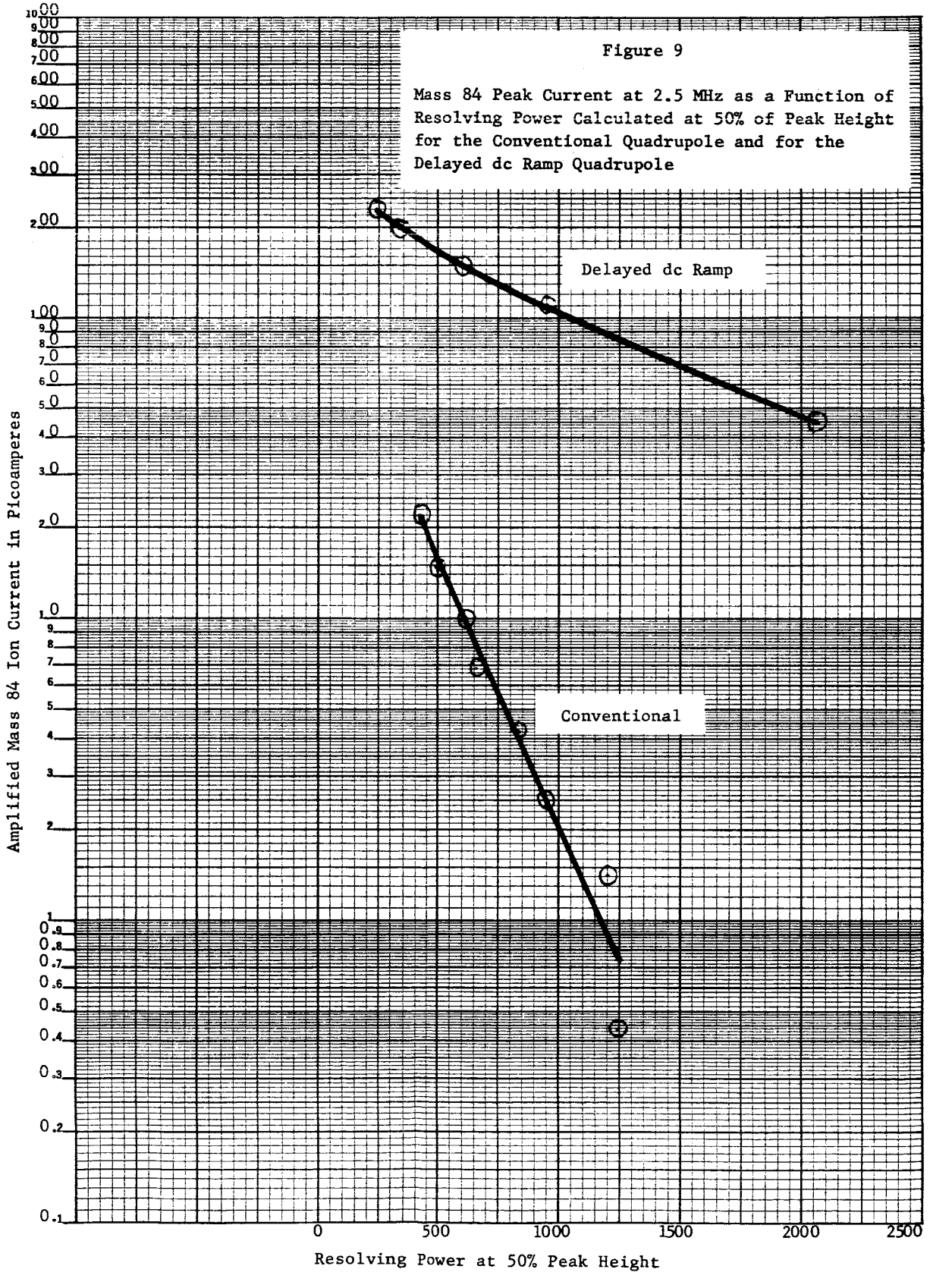

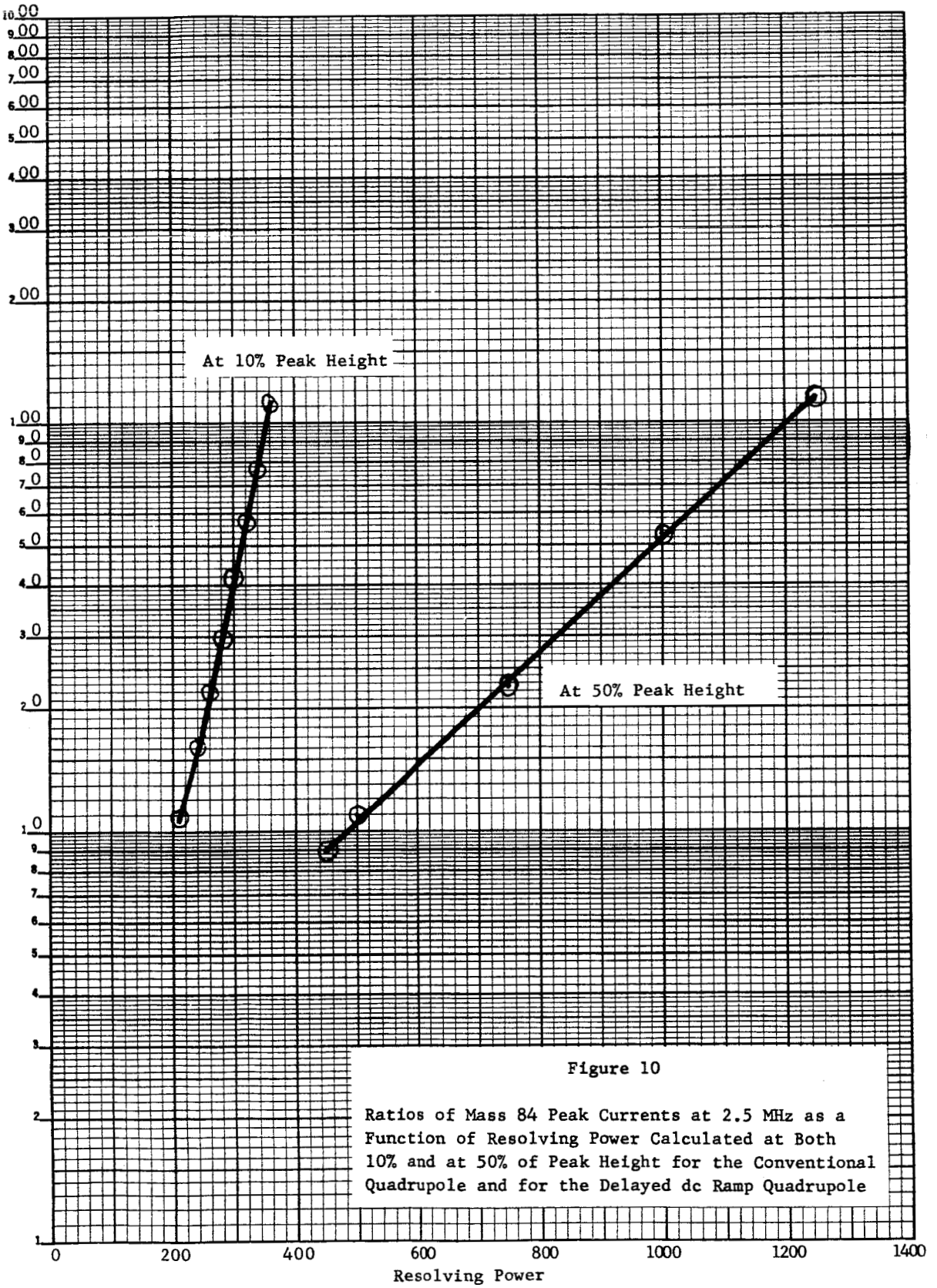

Figure 10

Ratios of Mass 84 Peak Currents at 2.5 MHz as a Function of Resolving Power Calculated at Both 10% and at 50% of Peak Height for the Conventional Quadrupole and for the Delayed dc Ramp Quadrupole